Genes to Cells

# PKCη deficiency improves lipid metabolism and atherosclerosis in apolipoprotein E-deficient mice

**Kumiko Torisu[1,2]*, Xueli Zhang[1], Mari Nonaka[1], Takahide Kaji[3], Daisuke Tsuchimoto[1,4], Kosuke Kajitani[1,5], Kunihiko Sakumi[1,4], Takehiro Torisu[2], Kazuhiro Chida[6], Katsuo Sueishi[7], Michiaki Kubo[8], Jun Hata[9], Takanari Kitazono[2], Yutaka Kiyohara[10] and Yusaku Nakabeppu[1,4]**

[1]*Division of Neurofunctional Genomics, Department of Immunobiology and Neuroscience, Medical Institute of Bioregulation, Kyushu University, 3-1-1 Maidashi, Higashi-ku, Fukuoka 812-8582, Japan*
[2]*Department of Medicine and Clinical Science, Graduate School of Medical Sciences, Kyushu University, 3-1-1 Maidashi, Higashi-ku, Fukuoka 812-8582, Japan*
[3]*Translational Research Department, Sohyaku, Innovative Research Division, Mitsubishi Tanabe Pharma Corporation, 17-10 Nihonbashi, Koami-cho, Chuo-ku, Tokyo 103-8405, Japan*
[4]*Research Center for Nucleotide Pool, Kyushu University, 3-1-1 Maidashi, Higashi-ku, Fukuoka 812-8582, Japan*
[5]*Counseling and Health Center, Faculty of Arts and Science, Kyushu University, 744 Motooka, Nishi-ku, Fukuoka 819-0395, Japan*
[6]*Department of Animal Resource Sciences, Graduate School of Agricultural and Life Sciences, The University of Tokyo, 1-1-1 Yayoi, Bunkyo-ku, Tokyo 113-8657, Japan*
[7]*Department of Pathology, Graduate School of Medical Sciences, Kyushu University, 3-1-1 Maidashi, Higashi-ku, Fukuoka 812-8582, Japan*
[8]*Laboratory for Genotyping Development, Center for Genomic Medicine, RIKEN 1-7-22 Suehiro-cho, Tsurumi-ku, Yokohama 230-0045, Japan*
[9]*Department of Epidemiology and Public Health, Graduate School of Medical Sciences, Kyushu University, 3-1-1 Maidashi, Higashi-ku, Fukuoka 812-8582, Japan*
[10]*Department of Environmental Medicine, Graduate School of Medical Sciences, Kyushu University, 3-1-1 Maidashi, Higashi-ku, Fukuoka 812-8582, Japan*

**Genomewide association studies have shown that a nonsynonymous single nucleotide polymorphism in *PRKCH* is associated with cerebral infarction and atherosclerosis-related complications. We examined the role of PKCη in lipid metabolism and atherosclerosis using apolipoprotein E-deficient ($Apoe^{-/-}$) mice. PKCη expression was augmented in the aortas of mice with atherosclerosis and exclusively detected in MOMA2-positive macrophages within atherosclerotic lesions. $Prkch^{+/+}Apoe^{-/-}$ and $Prkch^{-/-}Apoe^{-/-}$ mice were fed a high-fat diet (HFD), and the dyslipidemia observed in $Prkch^{+/+}Apoe^{-/-}$ mice was improved in $Prkch^{-/-}Apoe^{-/-}$ mice, with a particular reduction in serum LDL cholesterol and phospholipids. Liver steatosis, which developed in $Prkch^{+/+}Apoe^{-/-}$ mice, was improved in $Prkch^{-/-}Apoe^{-/-}$ mice, but glucose tolerance, adipose tissue and body weight, and blood pressure were unchanged. Consistent with improvements in LDL cholesterol, atherosclerotic lesions were decreased in HFD-fed $Prkch^{-/-}Apoe^{-/-}$ mice. Immunoreactivity against 3-nitrotyrosine in atherosclerotic lesions was dramatically decreased in $Prkch^{-/-}Apoe^{-/-}$ mice, accompanied by decreased necrosis and apoptosis in the lesions. ARG2 mRNA and protein levels were significantly increased in $Prkch^{-/-}Apoe^{-/-}$ macrophages. These data show that PKCη deficiency improves dyslipidemia and reduces susceptibility to atherosclerosis in $Apoe^{-/-}$ mice, showing that PKCη plays a role in atherosclerosis development.**

*Communicated by:* Shigeo Koyasu
**Correspondence:* torisuk@kcu.med.kyushu-u.ac.jp
*Conflict of interest:* The authors declare no conflict of interests.


DOI: 10.1111/gtc.12402

## Introduction

Stroke and ischemic heart disease are two of the leading causes of death worldwide. In genomewide association studies, the *PRKCH* gene, which encodes PKCη, has been reported as a novel susceptibility gene for atherosclerotic diseases such as cerebral infarction (Kubo *et al.* 2007; Serizawa *et al.* 2008; Cheng *et al.* 2009; Wu *et al.* 2009; Li *et al.* 2012). Previous studies established that there is a nonsynonymous single nucleotide polymorphism (SNP) in the *PRKCH* gene that is associated with increased risk of brain infarction and engenders increased PKCη activity (Kubo *et al.* 2007).

Protein kinase C (PKC) is a serine/threonine kinase activated by diacylglycerol, phospholipids and calcium. It regulates a wide variety of important cellular functions including proliferation, differentiation and apoptosis. There are three subgroups (classical, novel and atypical) in the PKC family. PKCη belongs to the novel PKC family. There is significant evidence linking PKCη to cellular differentiation (Ohba *et al.* 1998; Chida *et al.* 2003), cell cycle regulation (Fima *et al.* 2001), cell survival, malignant transformation and apoptosis (Griner & Kazanietz 2007). Recently, it was shown that the Toll-like receptor 4 (TLR4)–PKCη–phospholipase D2 pathway activates foam cell formation via down-regulation of the regulator of G protein signaling 2 (RGS2) (Lee *et al.* 2010), suggesting that PKCη participates in the development of atherosclerosis. It has also been shown that PKCη is expressed mainly in vascular endothelial cells and foamy macrophages in human atherosclerotic lesions, and its expression increases as the lesion type progresses (Kubo *et al.* 2007). However, there is no experimental evidence indicating that PKCη is involved in the pathology of atherosclerosis.

To verify whether deficiency of PKCη alters atherosclerosis progression, we compared PKCη/apolipoprotein E-double-deficient ($Prkch^{-/-}Apoe^{-/-}$) mice with apolipoprotein E-deficient ($Prkch^{+/+}Apoe^{-/-}$) mice. We report that $Prkch^{-/-}Apoe^{-/-}$ mice fed a high-fat diet (HFD) showed significantly ameliorated dyslipidemia with reduced atherosclerosis compared with $Prkch^{+/+}Apoe^{-/-}$ mice fed the same diet. These observations support an *in vivo* role for PKCη in the progression of atherosclerosis through regulation of serum lipid levels. Our results suggest that PKCη may be a novel therapeutic target for improving dyslipidemia in atherosclerosis.

## Results

### Increased PKCη expression in mouse atherosclerosis

To better understand how PKCη might contribute to atherosclerosis progression, we analyzed PKCη expression in mouse aorta. Western blotting showed that PKCη protein levels in atherosclerotic aorta tissues prepared from $Prkch^{+/+}Apoe^{-/-}$ mice fed HFD were significantly higher than those in mild atherosclerotic aorta from low-fat diet (LFD)-fed $Prkch^{+/+}Apoe^{-/-}$ mice or nonatherosclerotic aorta tissues from C57BL/6J mice fed a LFD (Fig. 1A). To analyze the localization of PKCη in mouse atherosclerosis, we carried out immunohistochemistry of PKCη in $Prkch^{+/+}Apoe^{-/-}$ and $Prkch^{-/-}Apoe^{-/-}$ mice (Fig. 1B). In HFD-fed $Prkch^{+/+}Apoe^{-/-}$ mice, a high level of PKCη immunoreactivity was observed on the plasma membrane of MOMA2-positive macrophages infiltrating the atherosclerotic lesions (Fig. 1B). Such immunoreactivity was completely abolished in $Prkch^{-/-}Apoe^{-/-}$ mice, which suggests that these signals are derived from a PKCη-specific signal. Among the various tissues from C57BL/6J that were examined, the level of *Prkch* mRNA determined by quantitative RT-PCR was highest in thioglycollate-induced peritoneal macrophages (Fig. 1C). The level of PKCη protein in macrophages was also the highest among the tissues examined, whereas lower levels of PKCη protein were detected in other tissues (Fig. 1D). It is noteworthy that the levels of PKCη proteins in both white adipose tissues (WAT) and brown adipose tissues (BAT) were very low, even though the levels of *Prkch* mRNA were approximately 60% of the levels in macrophages. Expression analysis of PKCη suggested the importance of PKCη in activated macrophages. To examine whether the severity of atherosclerosis affects PKCη expression in macrophages, we also examined PKCη protein levels in peritoneal macrophages prepared from wild-type C57BL/6J mice fed a LFD with no atherosclerosis and $Apoe^{-/-}$ mice fed a LFD with mild atherosclerosis or a HFD with severe atherosclerosis by Western blotting (Fig. 1E). ApoE deficiency increased PKCη expression in macrophages prepared from mice fed a LFD; however, PKCη expression decreased in macrophages from HFD-fed ApoE-deficient mice. These results suggest the functional importance of PKCη in macrophages.

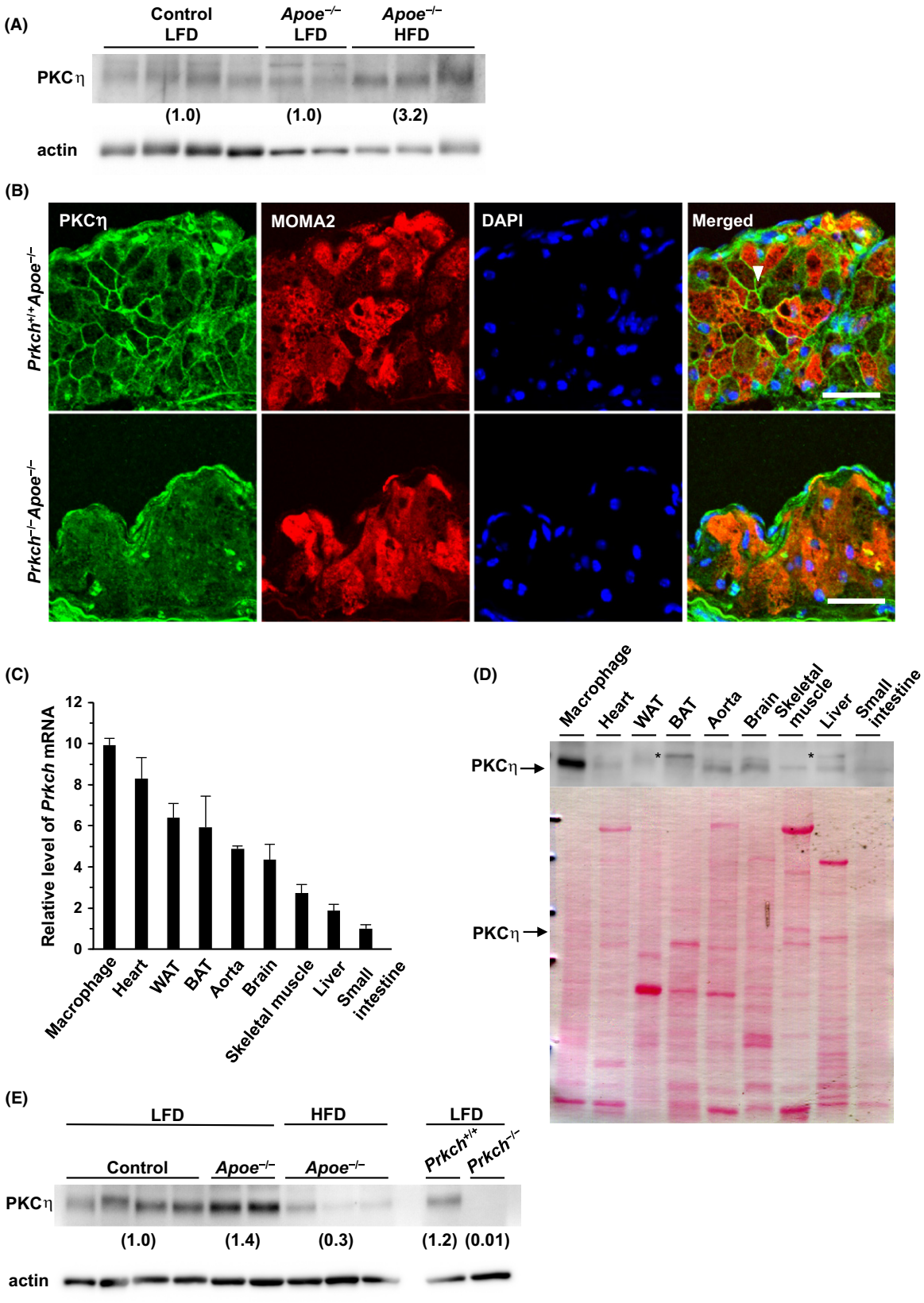

### Improved dyslipidemia and liver steatosis in *Prkch*$^{-/-}$*Apoe*$^{-/-}$ mice fed a HFD

To verify alteration of major risk factors for atherosclerosis in *Prkch*$^{+/+}$*Apoe*$^{-/-}$ and *Prkch*$^{-/-}$*Apoe*$^{-/-}$ mice, we first compared serum lipid profiles. HFD-induced dyslipidemia observed in *Prkch*$^{+/+}$*Apoe*$^{-/-}$ mice was significantly improved in *Prkch*$^{-/-}$*Apoe*$^{-/-}$ mice (Fig. 2). LDL cholesterol levels in *Prkch*$^{-/-}$*Apoe*$^{-/-}$ mice improved to 70.3% of the levels seen in *Prkch*$^{+/+}$ *Apoe*$^{-/-}$ mice (Fig. 2B), which is expected to suppress atherosclerosis progression. Additionally, the levels of triacylglycerol and phospholipids in *Prkch*$^{-/-}$*Apoe*$^{-/-}$ mice were 62.2% and 75.0% of the levels in *Prkch*$^{+/+}$ *Apoe*$^{-/-}$ mice, respectively (Fig. 2D and F).

Small, dense LDL particles are now considered a predictive factor for cardiovascular diseases, and the ratio of triglycerides to HDL cholesterol is linked to small, dense LDL particles (Miller *et al.* 2011); therefore, we calculated the triglycerides to HDL cholesterol ratio based on the data shown above. The obtained ratios were 5.8 in *Prkch*$^{+/+}$*Apoe*$^{-/-}$ and 3.2 in *Prkch*$^{-/-}$*Apoe*$^{-/-}$ mice. A ratio greater than 4 is the most powerful independent predictor of coronary artery diseases (da Luz *et al.* 2008); thus, these results indicate that PKCη deficiency decreases such risk.

Consistent with the improvement in serum triacylglycerol, HFD-induced liver steatosis was markedly attenuated in *Prkch*$^{-/-}$*Apoe*$^{-/-}$ mice (Fig. 3A). The mean intensity of Sudan IV staining in the livers of HFD-fed *Prkch*$^{-/-}$*Apoe*$^{-/-}$ mice was less than 50% of that in HFD-fed *Prkch*$^{+/+}$*Apoe*$^{-/-}$ mice (Fig. 3B).

Macrophages play an important role in the onset of hepatic steatosis; therefore, we counted the number of Kupffer cells in the liver. Kupffer cell density was significantly decreased in *Prkch*$^{-/-}$*Apoe*$^{-/-}$ livers compared with *Prkch*$^{+/+}$*Apoe*$^{-/-}$ livers (Fig. 3C and D). To evaluate inflammatory responses in the liver, we carried out microarray analysis of liver tissue samples. We found 486 genes exhibited a greater than 1.4-fold change in expression between *Prkch*$^{+/+}$*Apoe*$^{-/-}$ and *Prkch*$^{-/-}$*Apoe*$^{-/-}$ livers, and 99 genes were categorized as involved in 'inflammatory response' processes by the computational gene network prediction tool IPA. Among these, 64 genes exhibited average raw expression levels greater than 100 in one of the two samples. Although the level of *Alb*, which encodes a liver-specific protein, was unchanged in PKCη-deficient livers (average raw expression level: 19869.9 in *Prkch*$^{+/+}$ *Apoe*$^{-/-}$ and 21196.9 in *Prkch*$^{-/-}$*Apoe*$^{-/-}$, fold change = 1.07), most of the proinflammatory genes were down-regulated in *Prkch*$^{-/-}$*Apoe*$^{-/-}$ livers (Table S1 in Supporting Information), consistent with the decrease in the number of Kupffer cells in the liver. However, we found that serum levels of the proinflammatory cytokine IL-6 were unchanged between *Prkch*$^{+/+}$*Apoe*$^{-/-}$ and *Prkch*$^{-/-}$*Apoe*$^{-/-}$ mice (Fig. S2A in Supporting Information).

Because other PKC isozymes, such as PKCβ, are known to be involved in diabetes (Brownlee 2001), and hepatic steatosis is known to be associated with insulin resistance (Gaggini *et al.* 2013), we next examined levels of blood glucose and insulin. Neither

**Figure 1** Increased expression of PKCη in mouse atherosclerosis. (A) Western blot analysis of PKCη in mouse aorta. Upper panel, Western blot of PKCη; 5-month-old wild-type C57BL/6J male mice fed a LFD with no atherosclerosis (control LFD, $n = 4$); 5-month-old *Apoe*$^{-/-}$ male mice fed a LFD with mild atherosclerosis (*Apoe*$^{-/-}$ LFD, $n = 2$); 5-month-old *Apoe*$^{-/-}$ male mice fed a HFD for 12 weeks with severe atherosclerosis (*Apoe*$^{-/-}$ HFD 12w, $n = 3$). Lower panel, actin; β-actin is shown as an internal control. Mean values of the relative intensities of PKCη normalized to the intensity of β-actin are shown in parentheses. (B) Confocal immunofluorescence microscopic detection of PKCη in atherosclerotic lesions. Green, anti-PKCη antibody; red, MOMA2; blue, DAPI. The arrowhead indicates PKCη signals on the plasma membrane of MOMA2-positive cells within atherosclerotic lesions. Scale bar, 50 μm. (C) Quantification of *Prkch* mRNA in mouse tissues. Eight-week-old C57Bl/6J male mice were examined. The *Prkch* mRNA level is shown as a relative value normalized to the 18S ribosomal RNA level. Macrophages, thioglycollate-elicited peritoneal macrophages; WAT, white adipose tissue; BAT, brown adipose tissue. (D) Western blot analysis of PKCη in mouse tissues. The same tissues shown in (C) from 8-week-old C57Bl/6J male mice were examined. One representative experiment carried out in triplicate is shown. Upper panel, Western blot of PKCη; lower panel, Ponceau S-stained image of the blot to confirm equal loading of proteins (5 μg total protein per lane). The level of PKCη is the highest in macrophages; other tissues express much less PKCη. The arrow shows PKCη protein. *, nonspecific signal. (E) Western blot analysis of PKCη in murine peritoneal macrophages. Peritoneal macrophages were prepared from 5-month-old C57BL/6J male mice (Control LFD, $n = 4$); 5-month-old *Apoe*$^{-/-}$ male mice fed a LFD (*Apoe*$^{-/-}$ LFD, $n = 2$); 5-month-old *Apoe*$^{-/-}$ male mice fed a HFD for 12 weeks (*Apoe*$^{-/-}$ HFD, $n = 3$); 5-month-old *Prkch*$^{+/+}$ male mouse fed a LFD (*Prkch*$^{+/+}$ LFD, $n = 1$); 5-month-old *Prkch*$^{-/-}$ male mouse fed a LFD (*Prkch*$^{-/-}$ LFD, $n = 1$). Actin; β-actin is shown as an internal control. The relative intensities of PKCη normalized to the intensity of β-actin are shown in parentheses.

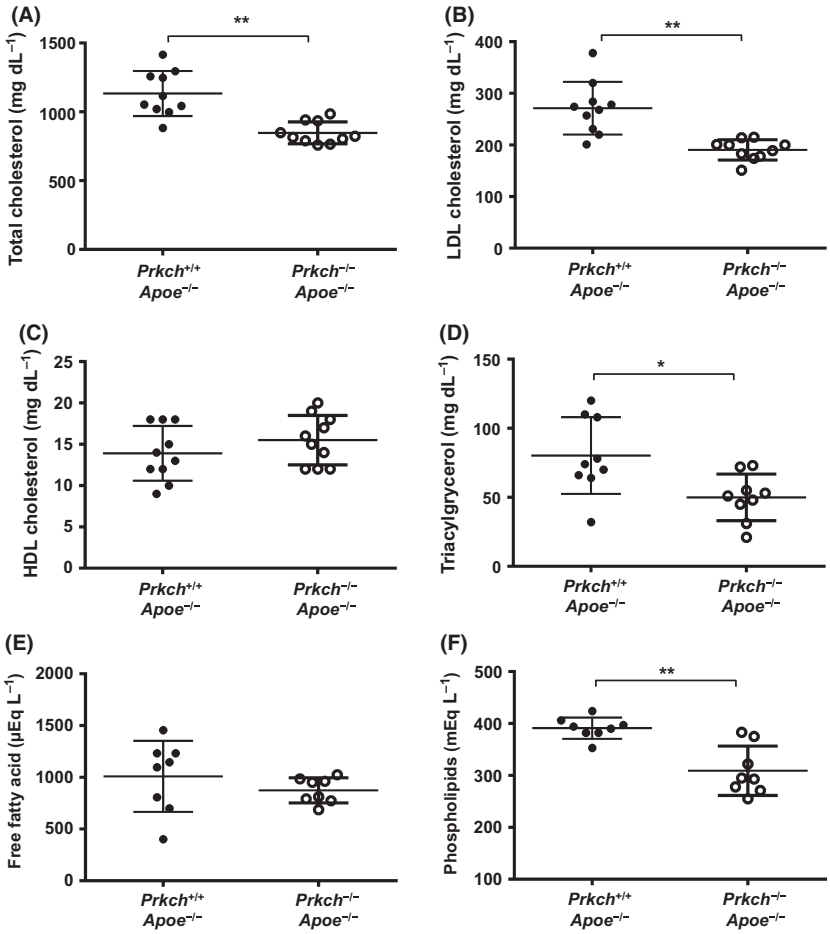


**Figure 2** Improved dyslipidemia in *Prkch*$^{-/-}$*Apoe*$^{-/-}$ mice fed a high-fat diet (HFD). (A–F) Metabolic serum profiles of HFD-fed *Prkch*$^{+/+}$*Apoe*$^{-/-}$ mice ($n$ = 8, 10) and HFD-fed *Prkch*$^{-/-}$*Apoe*$^{-/-}$ mice ($n$ = 10). In one experiment, all mice were examined under fed conditions (A–C). In a second experiment, HFD-fed *Prkch*$^{+/+}$*Apoe*$^{-/-}$ and *Prkch*$^{-/-}$*Apoe*$^{-/-}$ mice were examined under fasting conditions (D–F). We compared the levels of (A) total cholesterol, (B) LDL cholesterol, (C) HDL cholesterol, (D) triacylglycerol, (E) free fatty acids and (F) phospholipids using the Mann–Whitney $U$-test. A single asterisk indicates $P < 0.05$. A double asterisk indicates $P < 0.01$. No asterisk indicates a lack of statistical significance ($P > 0.05$). Closed circles, HFD-fed *Prkch*$^{+/+}$ *Apoe*$^{-/-}$ mice; open circles, HFD-fed *Prkch*$^{-/-}$*Apoe*$^{-/-}$ mice.

fasting blood glucose level nor homeostasis model assessment-estimated insulin resistance (HOMA-IR) was altered by PKCη deficiency (Fig. 3E and F). We did not find any differences in food consumption, body weight, and area or weight of white adipose tissue (Fig. 3G–J) between HFD-fed *Prkch*$^{+/+}$*Apoe*$^{-/-}$ and *Prkch*$^{-/-}$*Apoe*$^{-/-}$ mice. PKCη deficiency caused slight alterations in the expression levels of gluconeogenesis-associated genes, such as *Pck1* and *G6pc* (*Pck1*, average raw expression level: 6616.8 in *Prkch*$^{+/+}$*Apoe*$^{-/-}$ and 4799.8 in *Prkch*$^{-/-}$*Apoe*$^{-/-}$; *G6pc*, average raw expression level: 5727.0 in *Prkch*$^{+/+}$*Apoe*$^{-/-}$ and 6971.2 in *Prkch*$^{-/-}$*Apoe*$^{-/-}$; $n$ = 2) in the liver. There was also no difference in systolic blood pressure between the two genotypes (Fig. 3K).

We further examined the effects of PKCη deficiency on glucose tolerance test with LFD- or HFD-fed mice (Fig. S2B and C in Supporting Information). Both *Prkch*$^{+/+}$ and *Prkch*$^{-/-}$ mice fed a LFD exhibited essentially normal recovery of blood glucose within 2 h after glucose administration, but both *Prkch*$^{+/+}$ and *Prkch*$^{-/-}$ mice fed a HFD had higher levels of fasting blood glucose and exhibited sustained increased levels of blood glucose for 2 h, indicating insulin resistance.

 

### Improved dyslipidemia in the HFD-induced obesity *Prkch*$^{-/-}$ mouse model

Because *Apoe*$^{-/-}$ mice exhibit reduced body weight gain compared with wild-type mice, even on a HFD, they are not an ideal model for obesity. To understand the role of PKCη in lipid metabolism, we analyzed HFD-induced obesity in PKCη single-knockout mice. HFD-fed *Prkch*$^{-/-}$ mice showed a significant reduction in the level of phospholipids, to 72% of the level observed in *Prkch*$^{+/+}$ littermates (Fig. 4D). Other lipids also tended to be decreased in *Prkch*$^{-/-}$ mice (Fig. 4A–C). The body weight and white adipose tissue weight of *Prkch*$^{+/+}$ and *Prkch*$^{-/-}$ mice fed a HFD were similar (Fig. 4E and F). Although how PKCη regulates lipid metabolism remains unresolved, PKCη deficiency appears to improve dyslipidemia induced by HFD, regardless of the *Apoe* genotype.

### Attenuated atherosclerosis in *Prkch*$^{-/-}$*Apoe*$^{-/-}$ mice fed a HFD

To determine whether *Prkch*$^{-/-}$*Apoe*$^{-/-}$ mice with improved LDL cholesterol level exhibit reduced atherosclerosis, we analyzed aortas of *Prkch*$^{+/+}$*Apoe*$^{-/-}$ and *Prkch*$^{-/-}$*Apoe*$^{-/-}$ mice. En face analysis of the whole aorta showed that *Prkch*$^{-/-}$*Apoe*$^{-/-}$ mice exhibited significantly fewer Oil Red O-positive lesions than did *Prkch*$^{+/+}$*Apoe*$^{-/-}$ mice (Fig. 5A and B). In agreement with en face analysis, Elastica van Gieson (EVG) staining showed that the atherosclerotic area in the aortic root was significantly reduced in *Prkch*$^{-/-}$*Apoe*$^{-/-}$ mice (Fig. 5C and D). Quantification of the Sudan IV-positive area in the aortic root also showed a significant reduction in the degree of lipid-laden lesions in *Prkch*$^{-/-}$*Apoe*$^{-/-}$ mice (Fig. 5E and F).

Examination of the area of MOMA2-positive macrophages in atherosclerotic lesions showed that this was not affected by PKCη deficiency (Fig. 6A and B). A 'macrophage balance' between proinflammatory (M1) and anti-inflammatory (M2) macrophages plays a major role in the pathogenesis of atherosclerotic plaques and affects the evolution and complications of atherosclerosis (Mantovani *et al.* 2009). However, the ratios of inducible nitric oxide synthase (iNOS)-positive cells (a marker for M1 macrophage) and Ym-1-positive cells (a marker for M2 macrophage) to total macrophages (Mac-3 positive cells) in plaques were not significantly different between HFD-fed *Prkch*$^{+/+}$*Apoe*$^{-/-}$ and *Prkch*$^{-/-}$*Apoe*$^{-/-}$ mice (Fig. 6C–F). Although high expression of PKCη in activated macrophages is evident (Fig. 1B–E), we were not able to clarify the change of number or function in atherosclerotic macrophages in *Prkch*$^{-/-}$*Apoe*$^{-/-}$ mice using immunohistochemical methods.

### Decreased oxidative stress and apoptosis in atherosclerotic lesions in HFD-fed *Prkch*$^{-/-}$*Apoe*$^{-/-}$ mice

Nitrotyrosine is known to reflect nitric oxide (NO)-derived oxidant levels (Radi 2004), which are strongly associated with coronary artery disease (Shishehbor *et al.* 2003; Pacher *et al.* 2007). We therefore compared 3-nitrotyrosine levels in HFD-fed *Prkch*$^{+/+}$*Apoe*$^{-/-}$ and *Prkch*$^{-/-}$*Apoe*$^{-/-}$ mice. A strong signal for 3-nitrotyrosine immunoreactivity was observed in the intimal thickening, with the next strongest signal being in the tunica media of the aortas of *Prkch*$^{+/+}$*Apoe*$^{-/-}$ mice. The signal intensity of 3-nitrotyrosine immunoreactivity in the intimal thickening of *Prkch*$^{-/-}$*Apoe*$^{-/-}$ mice was significantly reduced compared with *Prkch*$^{+/+}$*Apoe*$^{-/-}$ mice (Fig. 7A and B). Consistent with the changes in 3-nitrotyrosine immunoreactivity, the area of the necrotic core in *Prkch*$^{-/-}$*Apoe*$^{-/-}$ mice was significantly decreased compared with that in *Prkch*$^{+/+}$*Apoe*$^{-/-}$ mice (Fig. 7C and D). The apoptotic area in atherosclerotic lesions determined using a TUNEL assay was also significantly reduced in *Prkch*$^{-/-}$*Apoe*$^{-/-}$ mice (Fig. 7E and F).

To investigate whether gene expression profiles of macrophages are altered by PKCη deficiency, and thus contribute to the decreased NO synthesis in the atherosclerotic lesion, we carried out microarray analysis using RNA prepared from thioglycollate-elicited peritoneal macrophages. There were more than 215 genes whose expression levels were altered (fold change > 1.2, multiple comparison $P < 0.05$) in response to PKCη deficiency, and only 12 genes exhibited average raw expression levels greater than 100 in one of the two samples (Table S2 in Supporting Information). Among those genes, the expression of *Arg*2, the gene encoding arginase 2, which converts L-arginine to ornithine and urea in the NO biosynthetic pathway, was most significantly increased (raw expression levels ($n = 3$): 219.7, 1006.7 and 399.3 in *Prkch*$^{-/-}$*Apoe*$^{-/-}$ and 76.6, 105.5 and 81.7 in *Prkch*$^{+/+}$*Apoe*$^{-/-}$), with a larger variance. The expression of other genes was less than twofold, with the exception of PKCη itself. Moreover, we confirmed that expression levels of three *Nos* genes (*Nos1*, *Nos2* and *Nos3*) were not altered at all by

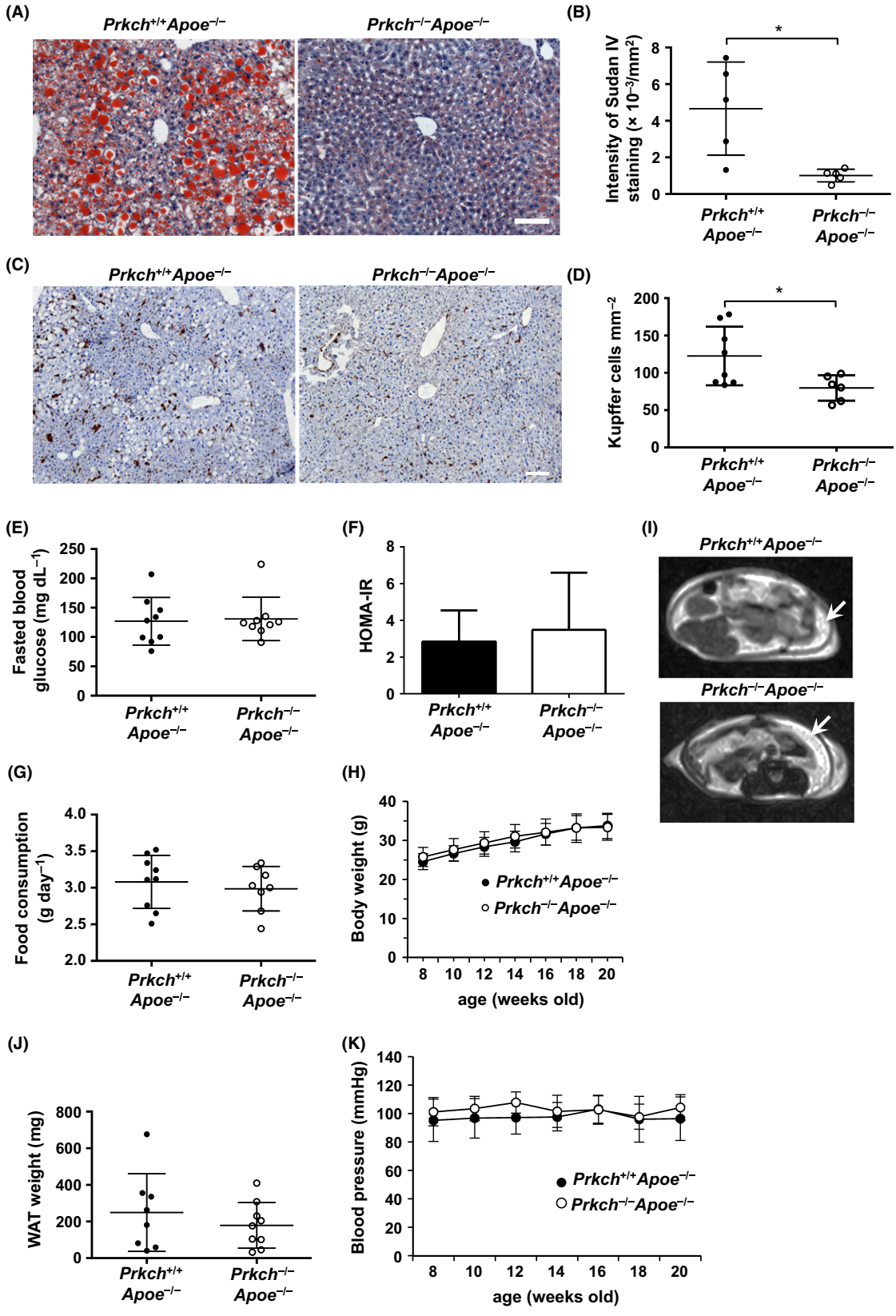

**Figure 3** Improved hepatosteatosis in *Prkch*$^{-/-}$*Apoe*$^{-/-}$ mice fed a high-fat diet. (A) Representative images of the liver stained by Sudan IV. Scale bar, 100 μm. (B) Quantification of Sudan IV-positive lipid droplets in the liver. Five mice of each genotype were examined. Closed circles indicate *Prkch*$^{+/+}$*Apoe*$^{-/-}$ mice; open circles, *Prkch*$^{-/-}$*Apoe*$^{-/-}$ mice. **P* = 0.013, unpaired *t*-test, two-tailed. (C) Immunohistochemical detection of MOMA2-positive Kupffer cells in the liver. Scale bar, 100 μm. (D) Density of Kupffer cells in the liver. The number of MOMA2-positive Kupffer cells per area (mm$^2$) is shown. Closed circles indicate *Prkch*$^{+/+}$ *Apoe*$^{-/-}$ mice (*n* = 8); open circles, *Prkch*$^{-/-}$*Apoe*$^{-/-}$ mice (*n* = 6). **P* = 0.02, unpaired *t*-test, two-tailed. (E) Fasting blood glucose levels. Mice fed a high-fat diet for 12 weeks, from 8 to 20 weeks of age, were fasted for 16 h and blood was then collected. Closed circles indicate *Prkch*$^{+/+}$*Apoe*$^{-/-}$ (*n* = 8); open circles indicate *Prkch*$^{-/-}$*Apoe*$^{-/-}$ mice (*n* = 8). (F) HOMA-IR in mice. HOMA-IR was calculated as follows: concentration of fasting insulin (μU/mL) × fasting glucose (mg/dL)/405. The closed bar indicates *Prkch*$^{+/+}$ *Apoe*$^{-/-}$ mice (*n* = 5); the open bar indicates *Prkch*$^{-/-}$*Apoe*$^{-/-}$ mice (*n* = 4). (G) Food consumption in mice. Daily food intake was measured from 16 to 20 weeks of age. Closed circles indicate *Prkch*$^{+/+}$*Apoe*$^{-/-}$ mice (*n* = 9); open circles indicate *Prkch*$^{-/-}$*Apoe*$^{-/-}$ mice (*n* = 8). (H) Body weight changes in *Apoe*$^{-/-}$ and *Prkch*$^{-/-}$*Apoe*$^{-/-}$ mice. Closed circles indicate *Prkch*$^{+/+}$*Apoe*$^{-/-}$ mice (*n* = 14); open circles, *Prkch*$^{-/-}$*Apoe*$^{-/-}$ mice (*n* = 16). (I) Magnetic resonance imaging of *Prkch*$^{+/+}$*Apoe*$^{-/-}$ and *Prkch*$^{-/-}$*Apoe*$^{-/-}$ mice. The arrow indicates white adipose tissue in the abdomen. (J) Weight of white adipose tissue (WAT). Right epididymal adipose tissue was weighed and plotted. Closed circles indicate *Prkch*$^{+/+}$*Apoe*$^{-/-}$ mice (*n* = 8); open circles, *Prkch*$^{-/-}$*Apoe*$^{-/-}$ (*n* = 9) mice. (K) Systolic blood pressure of mice. Blood pressure was measured in conscious mice by the tail-cuff method every 2 weeks. Closed circles indicate *Apoe*$^{-/-}$ (*n* = 13); open circles, *Prkch*$^{-/-}$*Apoe*$^{-/-}$ (*n* = 14) mice.

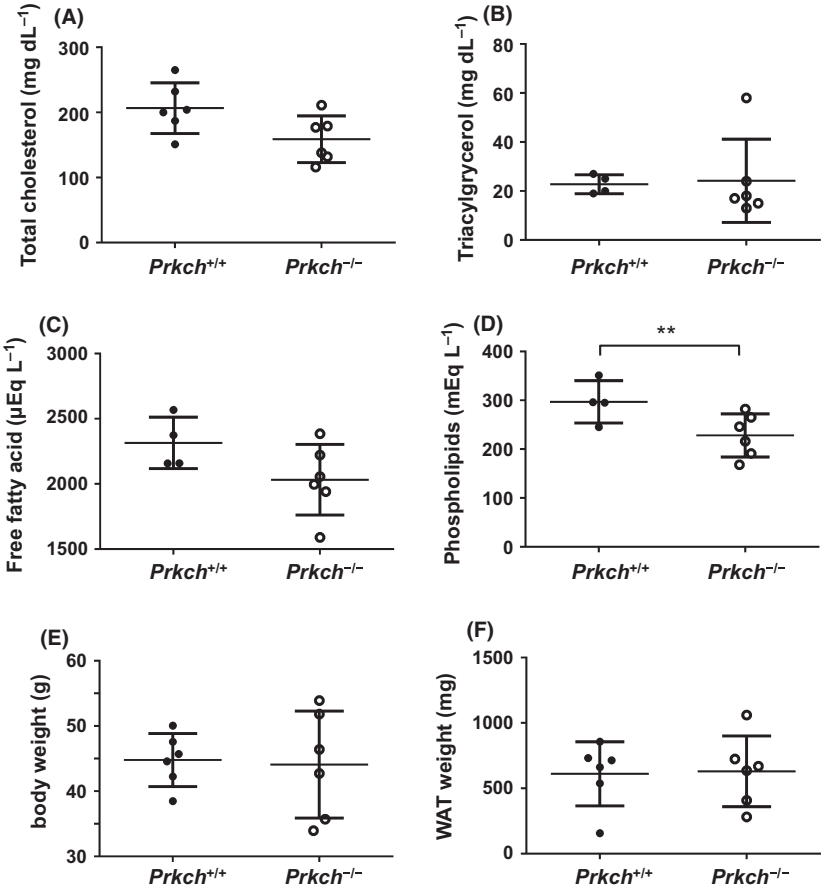


**Figure 4** Serum profiles of *Prkch*$^{-/-}$ mice and *Prkch*$^{+/+}$ littermates fed a high-fat diet. Mice were fed a high-fat diet for 22 weeks, from 8 to 30 weeks of age. Six mice of each genotype (A), or four *Prkch*$^{+/+}$ mice and six *Prkch*$^{-/-}$ mice (B–D) were examined under fasted conditions. (A) Total cholesterol, (B) triacylglycerol, (C) free fatty acids, (D) phospholipids. **P* = 0.01, unpaired *t*-test, two-tailed. (E) Body weights of *Prkch*$^{+/+}$ (*n* = 6) and *Prkch*$^{-/-}$ (*n* = 6) mice fed a high-fat diet. Body weight was measured at 30 weeks of age. (F) Weights of white adipose tissues (WAT). Right epididymal adipose tissue from *Prkch*$^{+/+}$ (*n* = 6) and *Prkch*$^{-/-}$ mice (*n* = 6) was weighed and plotted. **P* < 0.05, unpaired *t*-test, two-tailed. No asterisk indicates not statistically significant (*P* > 0.05). Closed circles indicate *Prkch*$^{+/+}$ mice; open circles, *Prkch*$^{-/-}$ mice.

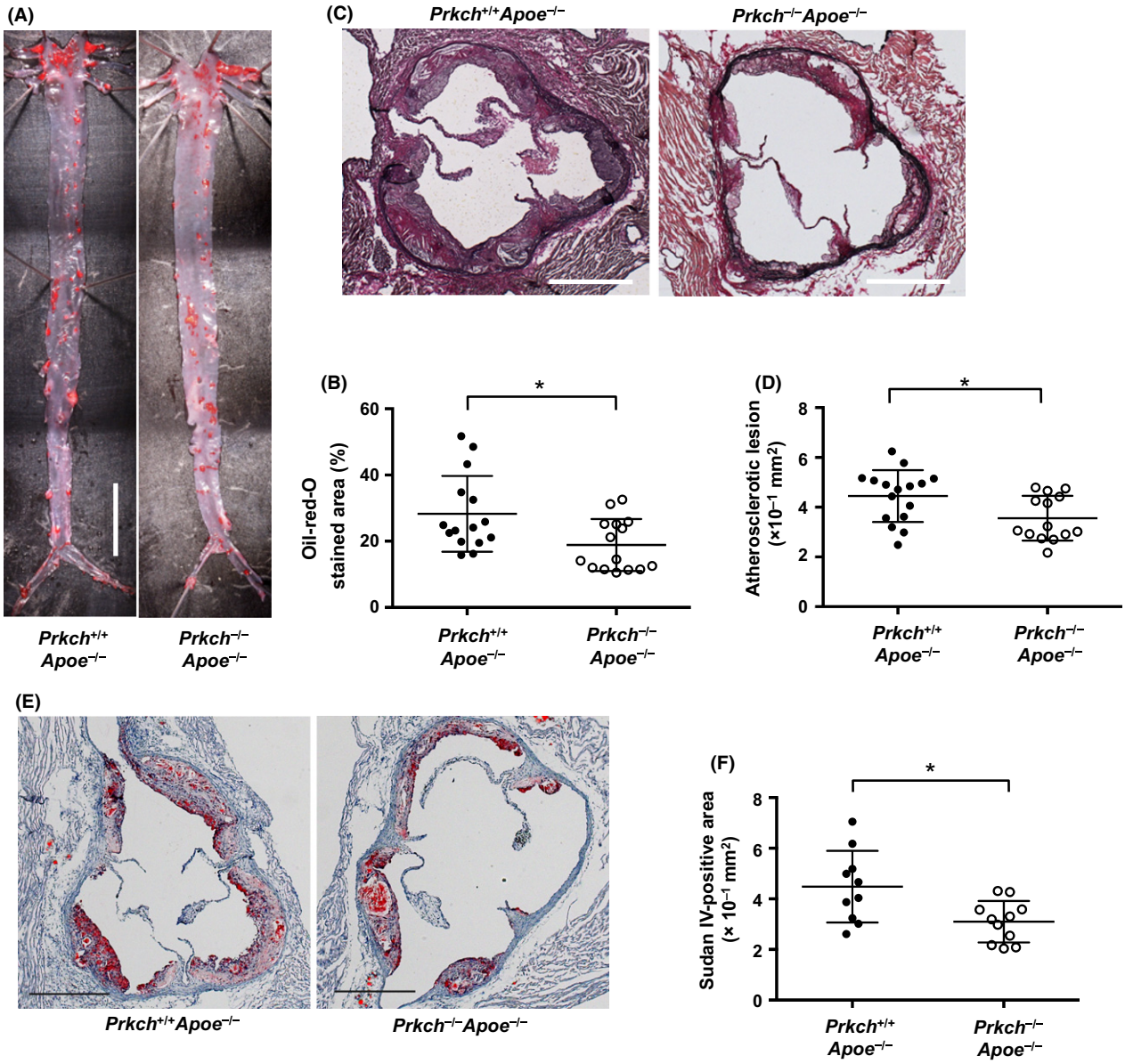


**Figure 5** Attenuated atherosclerosis in *Prkch*$^{-/-}$*Apoe*$^{-/-}$ mice fed a high-fat diet. (A) Representative images of whole aorta stained with Oil Red O. Scale bar, 0.5 cm. Mice fed a high-fat diet for 12 weeks, from 8 to 20 weeks of age, were examined. (B) Quantification of Oil Red O-positive lesions. The Oil Red O-stained area as a percentage of the total lumen area of the vessel is shown. The proximal region of the aorta covering 0.5 cm in length from the edge of the proximal aorta was analyzed. Closed circles indicate *Prkch*$^{+/+}$*Apoe*$^{-/-}$ mice ($n$ = 15); open circles, *Prkch*$^{-/-}$*Apoe*$^{-/-}$ mice ($n$ = 15). The means were 28.3% and 18.9%, respectively, and thus *Prkch*$^{-/-}$*Apoe*$^{-/-}$ mice showed an approximately 33% reduction in lesion area compared with *Prkch*$^{+/+}$*Apoe*$^{-/-}$ mice. *$P$ = 0.014, unpaired $t$-test, two-tailed. (C) Representative images of cross-sections of the aortic sinus. Each section was stained with EVG. Scale bar, 0.5 mm. (D) Quantification of the atherosclerotic area. Closed circles indicate *Prkch*$^{+/+}$*Apoe*$^{-/-}$ mice ($n$ = 16); open circles, *Prkch*$^{-/-}$*Apoe*$^{-/-}$ mice ($n$ = 14). The means of the area were 4.4 × $10^{-1}$ (*Prkch*$^{+/+}$*Apoe*$^{-/-}$) and 3.6 × $10^{-1}$ (*Prkch*$^{-/-}$*Apoe*$^{-/-}$) mm$^2$. *$P$ = 0.019, unpaired $t$-test, two-tailed. (E) Representative images of cross-sections of the aortic sinus stained by Sudan IV. Scale bar, 0.5 mm. (F) Quantification of the Sudan IV-positive area in atherosclerotic lesions. Closed circles indicate *Prkch*$^{+/+}$*Apoe*$^{-/-}$ mice ($n$ = 11); open circles, *Prkch*$^{-/-}$*Apoe*$^{-/-}$ mice ($n$ = 12). *$P$ = 0.038, unpaired $t$-test, two-tailed.

PKCη deficiency, supporting the iNOS immunostaining data shown in Fig. 6C.

*Arg2* mRNA expression was compared between peritoneal macrophages prepared from *Prkch*$^{+/+}$*Apoe*$^{-/-}$ and *Prkch*$^{-/-}$*Apoe*$^{-/-}$ mice by quantitative RT-PCR (Fig. 7G). The level of *Arg2* mRNA was fivefold higher in *Prkch*$^{-/-}$*Apoe*$^{-/-}$ macrophages than in *Prkch*$^{+/+}$*Apoe*$^{-/-}$ macrophages, confirming the results of the microarray data. Consistent with the increase in *Arg2* mRNA, ARG2 protein expression was significantly increased in *Prkch*$^{-/-}$*Apoe*$^{-/-}$ macrophages (Fig. 7H).

To examine the effects of increased ARG2 protein expression in macrophages, we introduced a human ARG2 (hARG2)-expressing plasmid into Raw264.7 cells, a murine macrophage cell line, and confirmed its expression without any treatment (Fig. 7I). LPS treatment induced the expression of the endogenous murine ARG2, and Raw264.7 cells expressing hARG2 had a 1.8-fold increase in ARG2 protein levels than those with the empty vector (control). After LPS treatment, nitrite and nitrate levels in the media were significantly increased in Raw264.7 cells with the empty vector, whereas nitrite and nitrate levels were significantly reduced in Raw264.7 cells expressing hARG2 (Fig. 7J), thus indicating that increased expression of ARG2 in macrophages attenuates the production of NO.

These results indicate that PKCη deficiency efficiently reduces oxidative stress and apoptosis in atherosclerotic lesions in HFD-fed *Prkch*$^{-/-}$*Apoe*$^{-/-}$ mice through the alteration of gene expression profiles, which result in reduced NO synthesis in macrophages.

## Discussion

In this study, we have showed for the first time that PKCη deficiency significantly improves dyslipidemia with reduced susceptibility to atherosclerosis, in the context of an *Apoe*-null background. Moreover, we found that PKCη deficiency decreases NO synthesis in macrophages, thus reducing 3-nitrotyrosine accumulation in the atherosclerotic lesions. Although we could not delineate the mechanism by which PKCη deficiency improves the dyslipidemia, our results indicate that PKCη plays an important role(s) in lipid metabolism as well as in regulation of macrophage function.

It has been established that a nonsynonymous SNP (1425G/A in exon 9 [rs2230500]) in the human *PRKCH* gene is related to susceptibility to cerebrovascular diseases (Kubo *et al.* 2007; Serizawa *et al.* 2008; Cheng *et al.* 2009; Wu *et al.* 2009; Li *et al.* 2012), rheumatoid arthritis (Takata *et al.* 2007) and gastric atrophy (Goto *et al.* 2010). The kinase activity of PKCη 374I, which is encoded by the *PRKCH* gene with the risk-type SNP (1425A), is significantly higher than that of PKCη-374V, which is encoded by the *PRKCH* gene with the SNP not associated with risk (1425G) (Kubo *et al.* 2007). In human atherosclerotic lesions, PKCη was shown to be expressed in CD68-positive macrophages, and its expression increased as the lesion type progressed (Kubo *et al.* 2007). In *Prkch*$^{+/+}$*Apoe*$^{-/-}$ mice fed a HFD for 12 weeks, we consistently confirmed that a high level of PKCη was expressed in macrophages infiltrating the atherosclerotic lesions (Fig. 1B). We thus consider that atherosclerosis developed under an *Apoe*-null background with HFD may be a suitable model to examine the effects of PKCη deficiency on atherosclerosis development.

In macrophage cell lines, PKCη and PKCδ are known to be translocated from the cytosol to the plasma membrane upon phorbol 12-myristate 13-acetate (TPA)-induced activation (Chen *et al.* 1997). In *Prkch*$^{+/+}$*Apoe*$^{-/-}$ mice, PKCη was mainly detected in the plasma membrane of MOMA2-positive macrophages within the atherosclerotic plaque (Fig. 1B), suggesting that PKCη detected in the macrophages might have been activated. It is known that oxidized LDL causes PKCα activation through sequential activation of Toll-like receptor (TLR) 4−spleen tyrosine kinase (Syk)−phospholipase C (PLC)γ (Bae *et al.* 2009; Levitan *et al.* 2010). Taken together, these results suggest that PKCη in *Prkch*$^{+/+}$*Apoe*$^{-/-}$ mice fed a HFD may also be activated upon exposure to oxidized LDL and thus chronically translocated to the plasma membrane of macrophages.

Aortic PKCη expression progressively increased as the atherosclerosis became more severe (Fig. 1A). This up-regulation of PKCη may reflect increased numbers of foamy macrophages and smooth muscle cells in the aorta, such as the MOMA2-positive and MOMA2-negative cells detected in Fig. 1B, thus reflecting the extent of atherosclerotic plaque formation, because smooth muscle cells in atherosclerotic plaques also express PKCη (Kubo *et al.* 2007). It has previously been shown that the area of the atherosclerotic lesion in the aortic arch is much larger (3 times or more) in HFD-fed *Apoe*$^{-/-}$ mice than in LFD-fed *Apoe*$^{-/-}$ mice (Wang *et al.* 2003). Accordingly, we observed higher PKCη levels in aortae from HFD-fed *Apoe*$^{-/-}$ mice than in aortae from

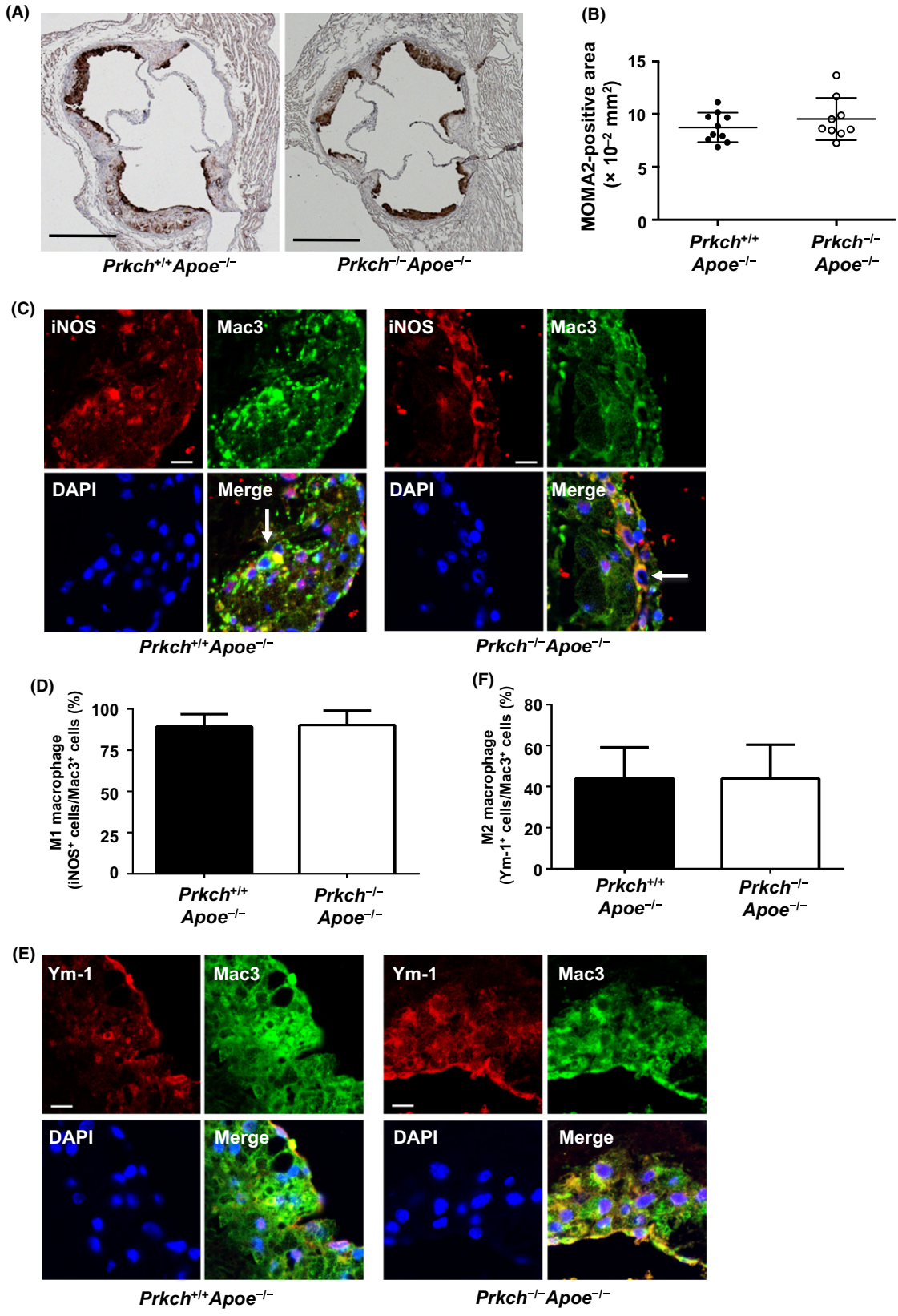

**Figure 6** MOMA2-positive area was not altered in *Prkch*$^{-/-}$*Apoe*$^{-/-}$ mice. (A) Immunohistochemical detection of MOMA2 within an atherosclerotic lesion. Scale bar, 0.5 mm. (B) Quantification of the MOMA2-positive area of atherosclerotic lesions from *Prkch*$^{+/+}$*Apoe*$^{-/-}$ and *Prkch*$^{-/-}$*Apoe*$^{-/-}$ mice. Closed circles indicate *Prkch*$^{+/+}$*Apoe*$^{-/-}$ mice ($n$ = 10); open circles, *Prkch*$^{-/-}$*Apoe*$^{-/-}$ mice ($n$ = 9) ($P$ = 0.32, unpaired $t$-test, two-tailed). (C) Immunohistochemical detection of iNOS and Mac3. Red, anti-iNOS; green, Mac3; blue, DAPI. (D) Ratio of iNOS-positive cells to Mac3-positive cells. Solid bar, *Prkch*$^{+/+}$*Apoe*$^{-/-}$ mice ($n$ = 5); open bar, *Prkch*$^{-/-}$*Apoe*$^{-/-}$ mice ($n$ = 5). (E) Immunostaining for Ym-1 and Mac3. Red, anti-Ym-1; green, Mac3; blue, DAPI. (F) Ratio of Ym-1-positive cells to Mac3-positive cells. Solid bar, *Prkch*$^{+/+}$*Apoe*$^{-/-}$ mice ($n$ = 5); open bar, *Prkch*$^{-/-}$*Apoe*$^{-/-}$ mice ($n$ = 5). Scale bar, 10 μm.

LFD-fed *Apoe*$^{-/-}$ mice (Fig. 1A). The heterogeneous cell population in aortae samples may explain the discrepancy in PKCη expression between aortae and isolated peritoneal macrophages (Fig. 1A, B and E).

PKC isoforms are known to be degraded via the ubiquitin-proteasome pathway following activation (Lu *et al.* 1998). This level of regulation is also applied to PKCη, which has been shown to be depleted after prolonged activation in Jurkat cells and osteoblasts (Schavinsky-Khrapunsky *et al.* 2003; Lampasso *et al.* 2006). In this study, we observed a down-regulation of PKCη in macrophages derived from HFD-fed *Apoe*$^{-/-}$ mice compared with those fed a LFD (Fig. 1E). This result could suggest that PKCη levels were decreased following prolonged activation by the excess lipids in HFD-fed *Apoe*$^{-/-}$ mice, and therefore activated PKCη in macrophages may be involved in atherosclerosis development.

We also attempted to examine the relationship between the severity of atherosclerosis and PKCη expression in aortae and isolated macrophages from *Apoe*$^{-/-}$ mice (Fig. 1A and E). However, other PKC isoforms are known to be closely related to insulin sensitivity, suggesting that the effect of a HFD on PKCη expression in wild-type C57Bl/6J mice should also be considered for these analyses.

It has been shown that the TLR4–PKCη–phospholipase D2 (PLD2) pathway activates foam cell formation via down-regulation of RGS2. Lee *et al.* (2010) showed that a PKCη pseudosubstrate completely attenuated LPS-induced foam cell formation, suggesting that PKCη deficiency suppresses atherosclerosis by decreasing foam cell formation. We observed a reduced Oil Red O-positive area in the en face aorta of *Prkch*$^{-/-}$*Apoe*$^{-/-}$ mice (Fig. 5A and B) and a smaller Sudan IV-positive area in aortic cross-sections (Fig. 5E and F), which may suggest decreased foam cell formation. Conversely, neither MOMA2-positive area nor M1/M2 balance was altered in *Prkch*$^{-/-}$*Apoe*$^{-/-}$ mice (Fig. 6A–F), thus suggesting that PKCη deficiency has much less impact on macrophage activation or polarization.

Reduction in 3-nitrotyrosine level in the atherosclerotic lesions by PKCη deficiency is likely a result of reduced peroxynitrite formation from NO in the activated macrophages (Fig. 7A and B), which may contribute to reduced necrosis or apoptosis in the atherosclerotic lesions (Fig. 7C–F) (Pacher *et al.* 2007). We found that ARG2 expression, in both mRNA and protein levels, was significantly increased in *Prkch*$^{-/-}$*Apoe*$^{-/-}$ macrophages (Fig. 7G and H, Table S2 in Supporting Information). Moreover, we showed that exogenous expression of human ARG2 in the murine macrophage cell line Raw264.7 significantly reduced LPS-induced NO synthesis (Fig. 7I and J). Arginase converts L-arginine to ornithine and urea, and L-arginine is an essential precursor for NO synthesis. It has been shown that ARG2-deficient peritoneal macrophages produce more NO when stimulated with bacteria *ex vivo* (Lewis *et al.* 2010), which is consistent with our observations. Our results thus suggest that in *Prkch*$^{-/-}$*Apoe*$^{-/-}$ macrophages, NO production is attenuated via depletion of arginine due to increased expression of the *Arg2* gene.

Ming *et al.* (2012) have reported that *Arg2*$^{-/-}$*Apoe*$^{-/-}$ mice displayed reduced atherosclerotic lesions with decreased macrophage inflammation compared with *Arg2*$^{+/+}$*Apoe*$^{-/-}$ mice. They also found that ARG2 deficiency improves insulin sensitivity, but had no effect on total plasma cholesterol or triglycerides, which are increased in *Arg2*$^{+/+}$*Apoe*$^{-/-}$ mice fed a HFD. Because ARG2 promotes the production of mitochondrial superoxide in LPS-treated macrophages, they concluded that ARG2 promotes proinflammatory responses in macrophage through mitochondrial superoxide. In this scenario, ARG2 may deplete cellular arginine, which is required for maintaining cellular or mitochondrial homeostasis (Mabalirajan *et al.* 2010; Changou *et al.* 2014).

It has been shown that superoxide and peroxynitrite produced by macrophages contribute to atherosclerosis progression. Macrophage-derived superoxides contribute to LDL oxidation (Cathcart 2004), while peroxynitrite derived from macrophages

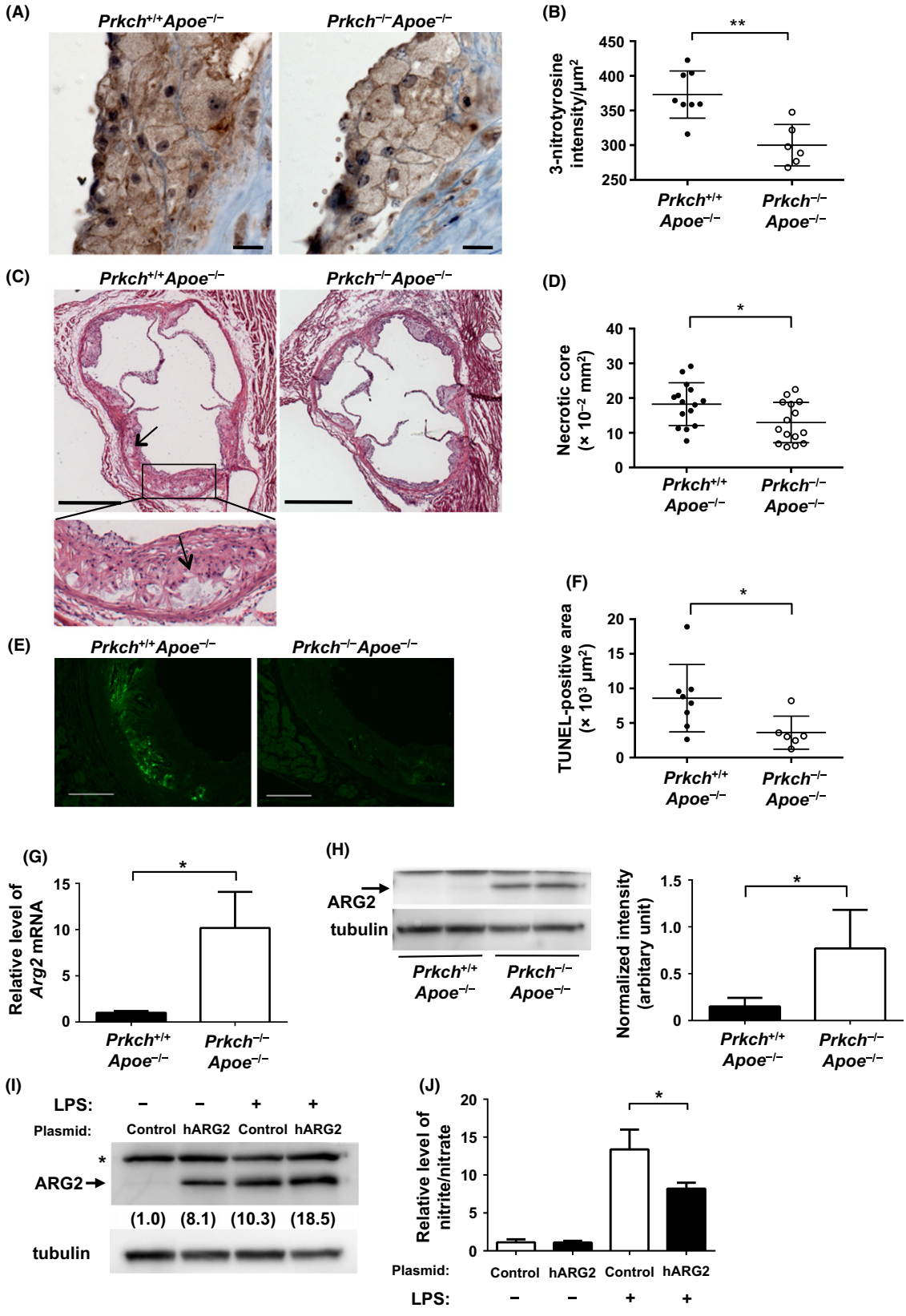

**Figure 7** Reduced oxidative stress and necrotic area in the atherosclerotic lesions of *Prkch*$^{-/-}$*Apoe*$^{-/-}$ mice. (A) Immunohistochemical detection of 3-nitrotyrosine in an atherosclerotic lesion. 3-Nitrotyrosine immunoreactivity was observed primarily in the intimal thickening. The *Prkch*$^{-/-}$*Apoe*$^{-/-}$ aorta showed lower 3-nitrotyrosine immunoreactivity compared with the *Prkch*$^{+/+}$ *Apoe*$^{-/-}$ aorta. Scale bar, 20 μm. (B) Quantification of 3-nitrotyrosine immunoreactivity in the intimal thickening. The intensity of immunoreactivity in the intimal thickening was selectively quantified. Closed circles indicate *Prkch*$^{+/+}$*Apoe*$^{-/-}$ mice ($n$ = 8); open circles, *Prkch*$^{-/-}$*Apoe*$^{-/-}$ mice ($n$ = 6). **$P$ = 0.001, unpaired $t$-test, two-tailed. (C) Hematoxylin and eosin staining of an atherosclerotic lesion. The arrow indicates the acellular area. Scale bar, 0.5 mm. (D) Quantification of the acellular area. Closed circles indicate *Prkch*$^{+/+}$*Apoe*$^{-/-}$ mice ($n$ = 15); open circles, *Prkch*$^{-/-}$*Apoe*$^{-/-}$ mice ($n$ = 15). *$P$ = 0.022, unpaired $t$-test, two-tailed. (E) Representative images of TUNEL assay result in atherosclerotic lesions. DNA strand breaks in lesions are labeled by terminal deoxynucleotidyltransferase. Scale bar, 50 μm. (F) Quantification of the TUNEL-positive area in atherosclerotic lesions. Closed circles indicate *Prkch*$^{+/+}$*Apoe*$^{-/-}$ mice ($n$ = 8); open circles, *Prkch*$^{-/-}$*Apoe*$^{-/-}$ mice ($n$ = 6). *$P$ = 0.041, unpaired $t$-test, two-tailed. (G) *Arg2* mRNA expression in macrophages. *Arg2* mRNA levels in thioglycollate-elicited peritoneal macrophages prepared from *Prkch*$^{+/+}$*Apoe*$^{-/-}$ and *Prkch*$^{-/-}$*Apoe*$^{-/-}$ mice were determined by quantitative RT-PCR. The *Arg2* mRNA level is shown as a relative value normalized to the 18S ribosomal RNA level. Closed box indicates *Prkch*$^{+/+}$*Apoe*$^{-/-}$ mice ($n$ = 4); open box, *Prkch*$^{-/-}$*Apoe*$^{-/-}$ mice ($n$ = 4). *$P$ = 0.03, Mann–Whitney $U$-test. (H) Expression of ARG2 protein in macrophages. One representative Western blot result is shown. ARG2 protein expression in thioglycollate-elicited peritoneal macrophages prepared from *Prkch*$^{+/+}$*Apoe*$^{-/-}$ and *Prkch*$^{-/-}$*Apoe*$^{-/-}$ mice was examined by Western blot. Upper panel, ARG2; lower panel, tubulin as an internal control (left panels). Intensity of ARG2 protein was quantified, normalized to tubulin and shown in a bar graph (right panel). Closed box, *Prkch*$^{+/+}$*Apoe*$^{-/-}$ mice ($n$ = 4); open box, *Prkch*$^{-/-}$*Apoe*$^{-/-}$ mice ($n$ = 5). *, $P$ = 0.02, Mann–Whitney $U$-test. (I) Exogenous expression of human ARG2 protein in the murine macrophage cell line. Raw264.7 cells were electroporated with a plasmid harboring the human ARG2 (hARG2) cDNA or an empty vector (control) and treated with or without LPS. ARG2 protein levels in the cells were examined by Western blot. Relative levels of ARG2 protein normalized to tubulin are shown in parentheses. *, nonspecific signal. (J) Reduced generation of nitrite and nitrate from hARG2-expressing macrophages. Relative levels of nitrite and nitrate in the medium were determined as described in the Cell culture paragraph of the Experimental procedures. In LPS-treated hARG2-expressing Raw264.7 cells, the level of nitrite and nitrate in the medium was reduced to 61.2% of the level seen in control cells. Closed box, control cells (nontreated and LPS-treated, $n$ = 4 each); open box, hARG2-overexpressing cells (nontreated and LPS-treated, $n$ = 4 each). *$P$ < 0.01, one-way ANOVA, Tukey's *post hoc* test.

modulates matrix degradation in atherosclerotic plaques (Rajagopalan *et al.* 1996). We suggested that HFD-fed *Arg2*$^{-/-}$*Apoe*$^{-/-}$ mice would increase NO production because of increased L-arginine levels; however, peroxynitrite levels may not be increased owing to the reduced mitochondrial superoxide. In contrast, HFD-fed *Prkch*$^{-/-}$*Apoe*$^{-/-}$ mice may produce increased levels of the superoxide; however, peroxynitrite levels may not be increased because of the reduced NO level. Therefore, we propose that PKCη deficiency significantly reduces the susceptibility to atherosclerosis in the *Apoe*-null background through the improved levels of LDL cholesterol and reduced peroxynitrite production.

ARG2 is required to establish insulin resistance in mice fed a HFD (Ming *et al.* 2012). We confirmed that PKCη deficiency does not alter the HFD-induced insulin resistance with or without ApoE deficiency (Figs 3E–H and S2B and C in Supporting Information), and this observation is consistent with the increased expression of ARG2 in PKCη-deficient macrophages.

Because PKCη deficiency effectively improved the dyslipidemia observed in HFD-fed *Prkch*$^{+/+}$*Apoe*$^{-/-}$ mice (Fig. 2), it is likely that the improvement in serum LDL cholesterol may contribute to reduced oxidized LDL cholesterol accumulation in macrophages from *Prkch*$^{-/-}$*Apoe*$^{-/-}$ mice (Fig. 5E and F), thus improving the atherosclerotic lesions. In *Prkch*$^{-/-}$ *Apoe*$^{-/-}$ mice fed a HFD, we conclude that the impact of PKCη deficiency on lipid metabolism was much stronger than any effect on macrophage function. It is interesting to note that PKCβ/ApoE double-knockout mice showed slightly lower levels of total serum cholesterol and triglycerides than did *Apoe* single-knockout mice (Harja *et al.* 2009). Zhu *et al.* (2012) reported that carriers of the 1425A SNP (GA + AA) have markedly high plasma LDL-C levels compared with GG carriers in a group of patients with coronary artery disease, but not in a control group.

It was recently reported that C/EBP β, which is a transcription factor that has a proinflammatory role in macrophages, is essential for systemic cholesterol balance. *Apoe*$^{-/-}$ mice reconstituted with C/EBP β-deficient bone marrow cells exhibited lower levels of serum LDL cholesterol and reduced atherosclerotic lesions compared with *Apoe*$^{-/-}$ mice reconstituted with wild-type bone marrow cells (Rahman *et al.* 2016). They also showed that C/EBP β deficiency in Raw264.7 macrophage cells prevented oxidized LDL-mediated foam cell formation and inflammatory cytokine production. Taken together, these data

suggest that macrophages regulate systemic lipid homeostasis and that increased activity of PKCη may disturb this regulatory function of macrophages, thereby contributing to increased serum LDL cholesterol levels. Further studies are needed to obtain direct experimental evidence for this hypothesis.

To explore the functional significance of PKCη in lipid metabolism during atherosclerosis development, various functional analyses of PKCη-deficient tissues are required. There is a study showed the importance of the PKCβ−early growth response-1 (Egr-1) pathway in endothelial cells. The PKCβ−Egr-1 axis plays a role not only in endothelial cells but also in diverse cell types including vascular smooth muscle cells, macrophages and lymphocytes, all of which are implicated in atherosclerosis (Yan *et al.* 2006). These studies suggest that each PKC isoform may play a unique role in atherosclerosis development. PKCη is known to be prominently expressed in the epithelia of the skin, digestive tract and respiratory tract in close association with epithelial differentiation (Osada *et al.* 1993). Because we could not show why whole-body dyslipidemia was improved by PKCη deficiency, tissue-specific knockout of the *Prkch* gene would help to identify target tissue(s) where expression of PKCη is essential to regulate serum lipid levels.

In summary, our results show that PKCη deficiency improved the dyslipidemia and atherosclerosis observed in HFD-fed $Apoe^{-/-}$ mice. Although PKCη may be involved in various cellular functions in addition to lipid metabolism, such as macrophage function, our result suggests that improvement of dyslipidemia is sufficient to reduce atherosclerosis. These results suggest that PKCη may be a new therapeutic target for improving dyslipidemia in atherosclerosis.

## Experimental procedures

### Mice

$Apoe^{-/-}$ mice were obtained from the Jackson Laboratory (Bar Harbor, ME, USA). $Prkch^{-/-}$ mice were established as previously described (Chida *et al.* 2003) (Fig. S1 in Supporting Information) and were backcrossed onto a C57BL/6J background for 13 generations. Colonies of $Prkch^{+/+}Apoe^{-/-}$ and $Prkch^{-/-}Apoe^{-/-}$ mice were established by inbred mating of $Prkch^{+/-}Apoe^{-/-}$ mice at the animal facilities of the Medical Institute of Bioregulation, Kyushu University. Mice were housed in plastic mouse cages and supplied with standard rodent chow (CA-1, Clea Japan, Tokyo, Japan) and water *ad libitum*. They were maintained in an air-conditioned specific pathogen-free room at 22 °C, with a 12:12-h light and dark cycle (lights on at 8:00 A.M., off at 8:00 P.M.). Genotyping was carried out as previously described (Chida *et al.* 2003). Male mice were weaned at 3 weeks of age and fed standard rodent chow as a LFD (CA-1, 5% of total calories from fat, Clea Japan Inc., Tokyo, Japan) for 5 weeks and were then changed to a HFD (custom diet, 40% of total calories from fat and 0.15% from cholesterol, Oriental Yeast Co., Tokyo, Japan). Mice were fed the HFD for 12 weeks, from 8 to 20 weeks of age, unless otherwise stated. Systolic blood pressure was measured every 2 weeks in conscious mice by the tail-cuff method using a model MK-2000ST blood pressure monitor for mice and rats (Muromachi Kikai, Tokyo, Japan). All animal experiments were approved by the Animal Care and Use Committee and the Biosafety Committee for Recombinant DNA experiments of Kyushu University, and carried out in accordance with the guidelines for Animal Experiments and Recombinant DNA Experiments, Kyushu University (Approval numbers, A18-005-2 and A25-233-0).

### Thioglycollate-elicited peritoneal macrophages

Two milliliters of 4% thioglycollate medium (Eiken Kagaku, Tokyo, Japan) was intraperitoneally injected into each mouse and, 4 days later, exudates were collected with ice-cold PBS. Collected cells were cultured in RPMI1640 (Life Technologies Japan, Ltd., Tokyo, Japan) supplemented with 10% FBS for 3 h. Dead cells were removed by washing with PBS three times and viable cells were used for further experiments.

### Cell culture

The murine macrophage cell line Raw264.7 was obtained from American Type Tissue Collection (Manassas, VA, USA). Cells were maintained at 37 °C, with 5% $CO_2$ in DMEM (Wako Chemicals, Osaka, Japan) supplemented with 10% FBS (Sigma-Aldrich, St. Louis, MO, USA), 100 U/mL penicillin and 100 mg/dL streptomycin (Life Technologies). Lipopolysaccharide (LPS) was purchased from Sigma-Aldrich. The mammalian expression vector pME18SFL3 harboring human ARG2 was obtained from Toyobo (Osaka, Japan). Cells were transfected with Cell Line Nucleofector kit V (Lonza Japan, Tokyo, Japan) and analyzed after 48 h of transfection. When indicated, cells were stimulated with 0.1 μg/mL LPS. The level of nitrite and nitrate in the medium was determined by Nitrate/Nitrite Colorimetric Assay Kit (Cayman Chemical, Ann Arbor, MI, USA).

### Tissue preparation and serum metabolic profile

Mice were anesthetized by intraperitoneal injection of 50 mg/kg sodium pentobarbital. After collection of blood from the vena cava, mice were perfused intracardially with 30 mL of saline followed by 30 mL of 4% paraformaldehyde (PFA). Isolated aorta and liver were further immersed in 4% PFA overnight, then cryoprotected by sequential treatment in 10% sucrose in PBS followed by 20% sucrose in PBS over 48 h at

 

4 °C. Tissues were then embedded in OCT compound (Sakura Finetek Japan, Tokyo, Japan) and immediately snap-frozen in liquid nitrogen and stored at −80 °C. Serum metabolic profiles were determined using commercial assay kits as follows: total cholesterol, L-type Wako CHO H; triacylglycerol, L-type Wako TG H; phospholipids, L-type Wako phospholipids; free fatty acid, NEFA-SS (Eiken Kagaku); LDL cholesterol, Cholestest LDL; HDL cholesterol, Cholestest NHDL (Sekisui Medical, Tokyo, Japan); glucose, Quick Auto Neo GLU-HK (Shino-Test Co., Kanagawa, Japan); insulin, Ultra-Sensitive Mouse Insulin ELISA kit (Morinaga Institute of Biological Sciences, Inc., Yokohama, Japan). Where indicated, mice were fasted for 16 h.

### Glucose tolerance test (GTT)

*Prkch*$^{+/+}$and *Prkch*$^{-/-}$ mice were fed a HFD for 12 weeks, from 8 to 20 weeks of age. After a 6-h fast, 2 g/kg body weight glucose was given intraperitoneally to the mice. Blood glucose concentrations were measured at 0, 15, 30, 60 and 90 min after glucose injection on a Freestyle FLASH glucometer (NIPRO, Osaka, Japan).

### Morphometric determination of atherosclerosis

For en face analysis, aorta tissue (including the proximal aorta and both iliac arteries) was stained with Oil Red O to determine the lesion area. The total and stained areas were quantified and the percentage of the surface area occupied by lesions was calculated from images acquired using a stereoscope equipped with a digital camera (Olympus, Tokyo, Japan) and software (IMAGEJ 1.42j, National Institutes of Health, Bethesda, MD, USA). To determine the cross-sectional lesion area, serial cross-sections (6 μm) of aortic root were prepared with a cryostat according to the method previously described (Ni *et al.* 2003). In brief, six levels within the aortic sinus region, separated by 120 μm with the most proximal site starting where the three aortic valves first appear, were examined. Using EVG-stained or Sudan IV-stained sections, the atherosclerotic area was quantified as previously described (Ni *et al.* 2003). Five levels within the aortic arch, separated by 120 μm, were quantified. Light field images were captured using an Axio Imager A1 microscope equipped with an AxioCamHRc camera (Carl Zeiss MicroImaging Japan, Tokyo, Japan). All images were analyzed using PHOTOSHOP 7.0 (Adobe, San Jose, CA, USA) and IMAGEJ 1.42j software.

### Antibodies used in this study

The following antibodies were used for immunohistochemical studies: rabbit polyclonal anti-mouse PKCη (400 ng/mL, sc-215, Santa-Cruz Biotechnology, Dallas, TX, USA), rat monoclonal antimonocyte/macrophage (MOMA2) (170 ng/mL, T-2007, Bachem, Bubendorf, Switzerland), mouse monoclonal anti-3-nitrotyrosine (1/100, clone 1A6, Millipore, Billerica, MA, USA), rabbit polyclonal anti-iNOS (20 μg/mL, ab3523, Abcam Japan, Tokyo, Japan), rabbit polyclonal anti-mouse Ym1 (1/50, #01404, StemCell Technologies, Vancouver, BC, Canada) and purified rat monoclonal anti-mouse Mac-3 (0.63 μg/mL, clone M3/84, BD Bioscience, San Jose, CA, USA). Respective nonimmune IgG (Dako Japan, Kyoto, Japan) was used as a negative control, and appropriate peroxidase-labeled secondary antibodies (Envision system, DAKO Japan) were used. For immunofluorescence microscopy, Alexa Fluor 488-conjugated goat anti-rabbit IgG (A1108), Alexa Fluor 594-conjugated donkey anti-rat IgG (A21209), Alexa Fluor 488-conjugated goat anti-mouse IgG (A10680), Alexa Fluor 594-conjugated goat anti-rabbit IgG (A11012) and Alexa Fluor 594-conjugated anti-mouse IgG (A11005) were used (Life Technologies).

### Immunostaining

For immunohistochemical analysis and immunofluorescence microscopy, air-dried cryostat sections (6 μm) were blocked with 3% nonfat milk, then incubated with a primary antibody followed by incubation with an appropriate peroxidase-labeled or fluorescence-conjugated secondary antibody. Light field images were captured using an Axio Imager A1 microscope equipped with an AxioCamHRc camera (Carl Zeiss MicroImaging Japan). Confocal images were acquired using an LSM510 META and LSM700 confocal microscope system (Carl Zeiss MicroImaging Japan). All images were analyzed using PHOTOSHOP 7.0 and IMAGEJ 1.42j software.

### TdT-mediated dUTP nick end labeling (TUNEL) assay

Paraffin-embedded aorta sections were used for TUNEL assays. Three sections from each mouse at the level of the aortic valve were examined. The TUNEL assay was carried out using the *in situ* Cell Death Detection Kit (Roche Diagnostics Japan, Tokyo, Japan), and the 3′-nick ends were labeled by incubating fluorescein-dUTP with terminal deoxynucleotidyl-transferase. Incorporated fluorescein-labeled dUTP was visualized using a fluorescence microscope (AxioSkop2 plus) equipped with a CCD camera (AxioCam) and AXIOVISION software (Carl Zeiss MicroImaging Japan). The TUNEL-positive area was measured using IMAGEJ 1.42j software.

### Real-time quantitative RT-PCR

Total RNA from mouse tissues was isolated using a combination of Isogen (Nippon Gene, Tokyo, Japan) and the RNeasy Mini kit (QIAGEN, Valencia, CA, USA). First-strand cDNAs were prepared using PrimeScript reverse transcriptase (Takara, Kyoto, Japan) and random primers. The relative levels of *Prkch* and *Arg2* mRNA were determined by real-time quantitative RT-PCR, according to a previously described method (Nonaka *et al.* 2009). 18S rRNA was used as an internal control.

The following primers were used: *Prkch* forward primer: 5′-GACCTGATGTTCCACATCCAAA; reverse primer: 5′-CGTGGTCCAATAGCACATTGTC; *Arg2* forward primer: 5′-CCCCTTTCTCTCGGGGACAGAA; reverse primer: 5′-GAAAGGAAAGTGGCTGTCCA; 18S rRNA forward primer: 5′-AGGATGTGAAGGATGGGAAG, reverse primer: 5′-ACGAAGGCCCCAAAAGTG.

### Western blot analysis

Mouse tissues were homogenized in ice-cold lysis buffer containing 125 mM Tris–HCl (pH 6.8), 10% glycerol, 4.0% SDS and protease inhibitor mixture (Nacalai Tesque, Kyoto, Japan). The homogenates were then centrifuged at 89 000 ***g*** for 30 min at 4 °C, and the supernatants collected. The protein concentration in the supernatant was measured using a DC protein assay kit (Bio-Rad Laboratories, Tokyo Japan). Equal amounts of total protein (5 μg) were separated by SDS-PAGE. Western blot analysis was carried out according to previously described methods (Tsuchimoto *et al.* 2001). The following primary antibodies were used for analysis: rabbit polyclonal anti-PKCη antibody (sc-215, Santa-Cruz Biotechnology), goat polyclonal anti-PKCη antibody (sc-215G, Santa-Cruz Biotechnology), goat polyclonal anti-arginase II antibody (sc-18357, Santa-Cruz Biotechnology), mouse monoclonal anti-β-actin antibody (Clone AC-74, Sigma-Aldrich) and rabbit polyclonal anti-α/β tubulin antibody (#2148, Cell Signaling). Digitized images were obtained using Ez-Capture MG (Atto, Tokyo, Japan), and the intensity of each band was quantified using CS ANALYZER version 3.0 software (Atto).

### IL-6 measurements

Murine serum IL-6 levels were measured using the mouse IL-6 Quantikine ELISA kit (R&D systems, Minneapolis, MN, USA) according to manufacturer's instructions.

### Mouse magnetic resonance imaging (MRI)

Mouse MRI was carried out as described previously (Tanaka *et al.* 2009). In brief, *in vivo* MRI scanning was carried out using a 0.3-T open MRI instrument (AIRIS II, Hitachi Medico, Tokyo, Japan) to determine body fat distribution. Mice were anesthetized with pentobarbital (50 mg/kg body weight) and placed in a coil. T1-weighted SE sequence (TR/TE = 450/14 ms; FOV 85 mm; matrix 512 × 512; slice thickness 2 mm) was used to acquire 14 transverse slices.

### Microarray analysis

Total RNA from mouse tissues was isolated using an RNeasy mini kit (QIAGEN). RNA quality was verified using a 2100 Bioanalyzer instrument (Agilent Technologies, Inc., Santa Clara, CA, USA). Gene expression in mouse tissues was analyzed using the GeneChip Mouse Gene 1.0 ST array (Affymetrix, Santa Clara, CA, USA). Sample preparation for microarray was carried out with an Affymetrix Mouse Gene 1.0ST Array kit according to the manufacturer's instruction. Arrays were scanned using the Affymetrix 3000 7G scanner and GENECHIP Operating Software version 1.4 to produce CEL intensity files.

### Statistics

Statistical analyses were carried out using the unpaired two-tailed Student's *t*-test or Mann–Whitney *U*-test. A *P* value less than or equal to 0.05 was considered significant. All values are expressed as mean ± SD.

## Acknowledgements

We are grateful to Dr T. Finkel (Center for Molecular Medicine, National Heart, Lung, and Blood Institute, Bethesda, MD) for his critical evaluation of our manuscript and for valuable suggestions. We thank Dr T. Sasaguri (Department of Clinical Pharmacology, Graduate School of Medical Sciences, Kyushu University), Dr S. Kanno (Department of Pediatrics, Graduate School of Medical Sciences, Kyushu University) and Dr H. Nishio (Center for the Study of Global Infection, Kyushu University Hospital) for providing the *Apoe*$^{-/-}$ mice, Mr H. Fujii, Dr T. Nakano (Department of Pathology, Faculty of Medicine, Kyushu University) and Ms S. Kitamura (Division of Neurofunctional Genomics, Department of Immunobiology and Neuroscience, Medical Institute of Bioregulation, Kyushu University) for immunohistochemistry and Ms S. Nishimura (Hitachi Medical Co., Tokyo, Japan) for mouse MRI.

This work was supported by grants from the Japan Society for the Promotion of Science (Grant-in-Aid for Scientific Research 20790535 to KT and 22221004 to YN) and Hisayama Research Institute for Lifestyle Disease, Fukuoka, Japan.

## References

Bae, Y.S., Lee, J.H., Choi, S.H., Kim, S., Almazan, F., Witztum, J.L. & Miller, Y.I. (2009) Macrophages generate reactive oxygen species in response to minimally oxidized low-density lipoprotein: toll-like receptor 4- and spleen tyrosine kinase-dependent activation of NADPH oxidase 2. *Circ. Res.* **104**, 210–218.

Brownlee, M. (2001) Biochemistry and molecular cell biology of diabetic complications. *Nature* **414**, 813–820.

Cathcart, M.K. (2004) Regulation of superoxide anion production by NADPH oxidase in monocytes/macrophages: contributions to atherosclerosis. *Arterioscler. Thromb. Vasc. Biol.* **24**, 23–28.

Changou, C.A., Chen, Y.R., Xing, L., Yen, Y., Chuang, F.Y., Cheng, R.H., Bold, R.J., Ann, D.K. & Kung, H.J. (2014) Arginine starvation-associated atypical cellular death involves mitochondrial dysfunction, nuclear DNA leakage,

 

and chromatin autophagy. *Proc. Natl Acad. Sci. USA* **111**, 14147–14152.

Chen, C.C., Wang, J.K. & Chen, W.C. (1997) TPA induces translocation but not down-regulation of new PKC isoform η in macrophages, MDCK cells and astrocytes. *FEBS Lett.* **412**, 30–34.

Cheng, H., Wang, F., Ding, X., Ding, H. & Song, X. (2009) Association of PRKCH gene with lacunar infarction in a local Chinese Han population. *Neurosci. Lett.* **464**, 146–149.

Chida, K., Hara, T., Hirai, T., Konishi, C., Nakamura, K., Nakao, K., Aiba, A., Katsuki, M. & Kuroki, T. (2003) Disruption of protein kinase Cη results in impairment of wound healing and enhancement of tumor formation in mouse skin carcinogenesis. *Cancer Res.* **63**, 2404–2408.

Fima, E., Shtutman, M., Libros, P., Missel, A., Shahaf, G., Kahana, G. & Livneh, E. (2001) PKCη enhances cell cycle progression, the expression of G1 cyclins and p21 in MCF-7 cells. *Oncogene* **20**, 6794–6804.

Gaggini, M., Morelli, M., Buzzigoli, E., DeFronzo, R.A., Bugianesi, E. & Gastaldelli, A. (2013) Non-alcoholic fatty liver disease (NAFLD) and its connection with insulin resistance, dyslipidemia, atherosclerosis and coronary heart disease. *Nutrients* **5**, 1544–1560.

Goto, Y., Hishida, A., Matsuo, K., Tajima, K., Morita, E., Naito, M., Wakai, K. & Hamajima, N. (2010) *PRKCH* gene polymorphism is associated with the risk of severe gastric atrophy. *Gastric Cancer* **13**, 90–94.

Griner, E.M. & Kazanietz, M.G. (2007) Protein kinase C and other diacylglycerol effectors in cancer. *Nat. Rev. Cancer* **7**, 281–294.

Harja, E., Chang, J.S., Lu, Y., Leitges, M., Zou, Y.S., Schmidt, A.M. & Yan, S.F. (2009) Mice deficient in PKCβ and apolipoprotein E display decreased atherosclerosis. *FASEB J.* **23**, 1081–1091.

Kubo, M., Hata, J., Ninomiya, T. *et al.* (2007) A nonsynonymous SNP in *PRKCH* (protein kinase Cη) increases the risk of cerebral infarction. *Nat. Genet.* **39**, 212–217.

Lampasso, J.D., Chen, W. & Marzec, N. (2006) The expression profile of PKC isoforms during MC3T3-E1 differentiation. *Int. J. Mol. Med.* **17**, 1125–1131.

Lee, H.K., Yeo, S., Kim, J.S., Lee, J.G., Bae, Y.S., Lee, C. & Baek, S.H. (2010) Protein kinase C-η and phospholipase D2 pathway regulates foam cell formation via regulator of G protein signaling 2. *Mol. Pharmacol.* **78**, 478–485.

Levitan, I., Volkov, S. & Subbaiah, P.V. (2010) Oxidized LDL: diversity, patterns of recognition, and pathophysiology. *Antioxid. Redox Signal.* **13**, 39–75.

Lewis, N.D., Asim, M., Barry, D.P., Singh, K., de Sablet, T., Boucher, J.L., Gobert, A.P., Chaturvedi, R. & Wilson, K.T. (2010) Arginase II restricts host defense to *Helicobacter pylori* by attenuating inducible nitric oxide synthase translation in macrophages. *J. Immunol.* **184**, 2572–2582.

Li, J., Luo, M., Xu, X. & Sheng, W. (2012) Association between 1425G/A SNP in PRKCH and ischemic stroke among Chinese and Japanese populations: a meta-analysis including 3686 cases and 4589 controls. *Neurosci. Lett.* **506**, 55–58.

Lu, Z., Liu, D., Hornia, A., Devonish, W., Pagano, M. & Foster, D.A. (1998) Activation of protein kinase C triggers its ubiquitination and degradation. *Mol. Cell. Biol.* **18**, 839–845.

da Luz, P.L., Favarato, D., Faria-Neto, J.R. Jr, Lemos, P. & Chagas, A.C. (2008) High ratio of triglycerides to HDL-cholesterol predicts extensive coronary disease. *Clinics (Sao Paulo)* **63**, 427–432.

Mabalirajan, U., Ahmad, T., Leishangthem, G.D., Dinda, A.K., Agrawal, A. & Ghosh, B. (2010) L-arginine reduces mitochondrial dysfunction and airway injury in murine allergic airway inflammation. *Int. Immunopharmacol.* **10**, 1514–1519.

Mantovani, A., Garlanda, C. & Locati, M. (2009) Macrophage diversity and polarization in atherosclerosis: a question of balance. *Arterioscler. Thromb. Vasc. Biol.* **29**, 1419–1423.

Miller, M., Stone, N.J., Ballantyne, C. *et al.* (2011) Triglycerides and cardiovascular disease: a scientific statement from the American Heart Association. *Circulation* **123**, 2292–2333.

Ming, X.F., Rajapakse, A.G., Yepuri, G., Xiong, Y., Carvas, J.M., Ruffieux, J., Scerri, I., Wu, Z., Popp, K., Li, J., Sartori, C., Scherrer, U., Kwak, B.R., Montani, J.P. & Yang, Z. (2012) Arginase II promotes macrophage inflammatory responses through mitochondrial reactive oxygen species, contributing to insulin resistance and atherogenesis. *J. Am. Heart Assoc.* **1**, e000992.

Ni, W., Tsuda, Y., Takashima, S., Sato, H., Sato, M. & Imaizumi, K. (2003) Anti-atherogenic effect of soya and rice-protein isolate, compared with casein, in apolipoprotein E-deficient mice. *Br. J. Nutr.* **90**, 13–20.

Nonaka, M., Tsuchimoto, D., Sakumi, K. & Nakabeppu, Y. (2009) Mouse RS21-C6 is a mammalian 2′-deoxycytidine 5′-triphosphate pyrophosphohydrolase that prefers 5-iodocytosine. *FEBS J.* **276**, 1654–1666.

Ohba, M., Ishino, K., Kashiwagi, M., Kawabe, S., Chida, K., Huh, N.H. & Kuroki, T. (1998) Induction of differentiation in normal human keratinocytes by adenovirus-mediated introduction of the η and δ isoforms of protein kinase C. *Mol. Cell. Biol.* **18**, 5199–5207.

Osada, S., Hashimoto, Y., Nomura, S., Kohno, Y., Chida, K., Tajima, O., Kubo, K., Akimoto, K., Koizumi, H., Kitamura, Y., Suzuki, K., Ohno, S. & Kuroki, T. (1993) Predominant expression of nPKCη, a Ca(2+)-independent isoform of protein kinase C in epithelial tissues, in association with epithelial differentiation. *Cell Growth Differ.* **4**, 167–175.

Pacher, P., Beckman, J.S. & Liaudet, L. (2007) Nitric oxide and peroxynitrite in health and disease. *Physiol. Rev.* **87**, 315–424.

Radi, R. (2004) Nitric oxide, oxidants, and protein tyrosine nitration. *Proc. Natl Acad. Sci. USA* **101**, 4003–4008.

Rahman, S.M., Baquero, K.C., Choudhury, M., Janssen, R.C., de la Houssaye, B.A., Sun, M., Miyazaki-Anzai, S., Wang, S., Moustaid-Moussa, N., Miyazaki, M. & Friedman, J.E. (2016) C/EBPβ in bone marrow is essential for diet

induced inflammation, cholesterol balance, and atherosclerosis. *Atherosclerosis* **250**, 172–179.

Rajagopalan, S., Meng, X.P., Ramasamy, S., Harrison, D.G. & Galis, Z.S. (1996) Reactive oxygen species produced by macrophage-derived foam cells regulate the activity of vascular matrix metalloproteinases in vitro. Implications for atherosclerotic plaque stability. *J. Clin. Invest.* **98**, 2572–2579.

Schavinsky-Khrapunsky, Y., Huleihel, M., Aboud, M. & Torgeman, A. (2003) Role of protein kinase C and the Sp1-p53 complex in activation of $p21^{WAF-1}$ expression by 12-*O*-tetradecanoylphorbol-13-acetate in human T cells. *Oncogene* **22**, 5315–5324.

Serizawa, M., Nabika, T., Ochiai, Y., Takahashi, K., Yamaguchi, S., Makaya, M., Kobayashi, S. & Kato, N. (2008) Association between *PRKCH* gene polymorphisms and subcortical silent brain infarction. *Atherosclerosis* **199**, 340–345.

Shishehbor, M.H., Aviles, R.J., Brennan, M.L., Fu, X., Goormastic, M., Pearce, G.L., Gokce, N., Keaney, J.F. Jr, Penn, M.S., Sprecher, D.L., Vita, J.A. & Hazen, S.L. (2003) Association of nitrotyrosine levels with cardiovascular disease and modulation by statin therapy. *JAMA* **289**, 1675–1680.

Takata, Y., Hamada, D., Miyatake, K., Nakano, S., Shinomiya, F., Scafe, C.R., Reeve, V.M., Osabe, D., Moritani, M., Kunika, K., Kamatani, N., Inoue, H., Yasui, N. & Itakura, M. (2007) Genetic association between the *PRKCH* gene encoding protein kinase Cη isozyme and rheumatoid arthritis in the Japanese population. *Arthritis Rheum.* **56**, 30–42.

Tanaka, R., Miwa, Y., Mou, K., Tomikawa, M., Eguchi, N., Urade, Y., Takahashi-Yanaga, F., Morimoto, S., Wake, N. & Sasaguri, T. (2009) Knockout of the *l-pgds* gene aggravates obesity and atherosclerosis in mice. *Biochem. Biophys. Res. Commun.* **378**, 851–856.

Tsuchimoto, D., Sakai, Y., Sakumi, K., Nishioka, K., Sasaki, M., Fujiwara, T. & Nakabeppu, Y. (2001) Human APE2 protein is mostly localized in the nuclei and to some extent in the mitochondria, while nuclear APE2 is partly associated with proliferating cell nuclear antigen. *Nucleic Acids Res.* **29**, 2349–2360.

Wang, H., Jiang, X., Yang, F., Gaubatz, J.W., Ma, L., Magera, M.J., Yang, X., Berger, P.B., Durante, W., Pownall, H.J. & Schafer, A.I. (2003) Hyperhomocysteinemia accelerates atherosclerosis in cystathionine β-synthase and apolipoprotein E double knock-out mice with and without dietary perturbation. *Blood* **101**, 3901–3907.

Wu, L., Shen, Y., Liu, X., Ma, X., Xi, B., Mi, J., Lindpaintner, K., Tan, X. & Wang, X. (2009) The 1425G/A SNP in *PRKCH* is associated with ischemic stroke and cerebral hemorrhage in a Chinese population. *Stroke* **40**, 2973–2976.

Yan, S.F., Harja, E., Andrassy, M., Fujita, T. & Schmidt, A.M. (2006) Protein kinase C β/early growth response-1 pathway: a key player in ischemia, atherosclerosis, and restenosis. *J. Am. Coll. Cardiol.* **48**, A47–A55.

Zhu, J., Yan, J.J., Kuai, Z.P., Gao, W., Tang, J.J., Jia, E.Z., Yang, Z.J. & Wang, L.S. (2012) The role of PRKCH gene variants in coronary artery disease in a Chinese population. *Mol. Biol. Rep.* **39**, 1777–1782.

*Received*: 5 September 2014
*Accepted*: 13 July 2016

## Supporting Information

Additional Supporting Information may be found online in the supporting information tab for this article:

**Figure S1** *Prkch* genotyping using tail DNA from $Prkch^{+/+}$ $Apoe^{-/-}$ ($Prkch^{+/+}$), $Prkch^{+/-}Apoe^{-/-}$ ($Prkch^{+/-}$) and $Prkch^{-/-}$ $Apoe^{-/-}$ ($Prkch^{-/-}$) mice.

**Figure S2** Serum IL6 levels and insulin resistance are not influenced by PKCη deficiency.

**Table S1** Altered expression of inflammatory response genes in $Prkch^{-/-}Apoe^{-/-}$ liver

**Table S2** Altered gene expression in macrophages from $Prkch^{-/-}Apoe^{-/-}$ mice

 